Tool Degradation Characterization in the Friction Stir Welding of Hard Metals

Microstructural characterization identified tool-life degrading mechanisms for three tungsten-based FSW tool materials

BY B. THOMPSON AND S. S. BABU

ABSTRACT

In recent years, friction stir welding (FSW) has made significant strides in the joining of hard metals such as steel and titanium thanks to advancements in tool materials. While the joining of hard metals using FSW shows significant promise with these advanced tool materials, a limiting factor remains tool life. The combination of high welding temperatures and flow stresses in the FSW of hard metals causes significant degradation of the tool. Previous tool degradation studies have defined observed types of wear or tracked dimensionally how much a tool material has degraded. Understanding tool degradation on a microstructural level would lead to the development of improved tool materials thereby increasing the opportunity for FSW to be employed as a joining method for hard metals. This study characterized the pre- and postweld microstructures of three tungsten-based tool materials: Material A (99% W-1% La_2O_3), Material B (75% W-25% Re), and Material C (70% W-20% Re-10% HfC). Tool degradation mechanisms were identified for each tool material based upon this characterization. Material A degraded by severe plastic deformation, Material B degraded by twinning, and Material C degraded by intergranular failure.

Introduction

Previous works examining tool degradation focused primarily on gross geometric changes a tool experienced during welding (Refs. 1–3). These changes were identified as both plastic deformation and tool wear; tool wear in this case specifying material loss. Wei Gan et al. investigated the friction stir welding (FSW) of L80 steel and demonstrated that two types of effects, deformation and wear, are main contributors to tool degradation (Ref. 4). Weinberger et al. also concluded that the limiting factors for FSW tools in hard metals are wear (abrasive and adhesive), brittle fracture, and deformation (Ref. 5).

Bentley et al. investigated deformation in tungsten (W) heavy alloys fabricated by powder metallurgy. These W-based microstructures were reported to fail by two main modes: cleavage or W-W grain boundary decohesion. Which type dominated depended upon material processing conditions. However, in W microstructures where the strain threshold had been reached (approximately 70% deformation), the W grains failed by cleavage mode because they could not withstand any more plastic deformation (Ref. 6).

Due to the complexity of describing how a tool material deteriorates during welding, the term tool degradation was concluded to be the best term to describe any loss of tool material integrity as a result of the FSW process. Tool degradation consists of two major components: wear and deformation. Tool wear describes material loss and includes abrasive and adhesive wear. Abrasive wear occurs as the tool material experiences the stresses of the welding environment. Particles of the tool material will, in effect, be lost to the welded material. Adhesive wear occurs when the material that is being welded adheres to the surface of the tool. In these areas a high stress concentration occurs, promoting material loss (Ref. 7). Plastic deformation is the second component of tool degradation. Types of plastic deformation that can occur in a FSW tool material include slipping or twinning. Oftentimes, plastic deformation is the most prominent cause of gross geometric changes in FSW tools (Refs. 4, 5, 8).

While these works (Refs. 1–8) provided valuable insight into characterizing the types of degradation FSW tools undergo and their geometrical changes, they did not investigate the microstructural changes that occur in the tool material during welding. By understanding how the microstructure of the tool material changes due to the FSW process, degradation mechanisms can be identified. A better understanding of these tool degradation mechanisms will lead to improved tool materials and/or tool designs, more appropriate tool material selection, and improved welding performance.

The three W-based alloys were chosen to best represent a wide range of W-based refractory alloys. The goal of this work was to investigate the microstructural changes the material experiences during welding and relate these changes to tool degradation. The tool materials were purposely welded under conditions designed to exacerbate the various mechanisms of degradation. In this way, the study represents "worst-case" weld quality conditions and provides the best case conditions to study degradation mechanisms.

KEYWORDS

Friction Stir Welding
Tool Materials
Tool Degradation
Wear
Deformation

Approach

Materials

The specific tool materials selected for microstructural characterization are three refractory-based alloys labeled Materials A, B, and C. Material A is made by doping pure W with 1.0 wt-% La_2O_3. This has the effect of increasing the creep strength and recrystallization temperature. Materials B and C are mainly comprised of W and rhenium (Re). Material B is specifically comprised of 75% W and 25% Re. The Re addition to the W has the effect of increasing the recrystallization temperature, ductility, and ultimate tensile strength. The Re also refines the microstructure and reduces the ductile-to-brittle transition temperature to –50°C (–58°F). These strengthening and hardening effects are

B. THOMPSON (bthompso@ewi.org) *is with Edison Welding Institute, Columbus, Ohio, and S. S. BABU is with The Ohio State University, Columbus, Ohio.*

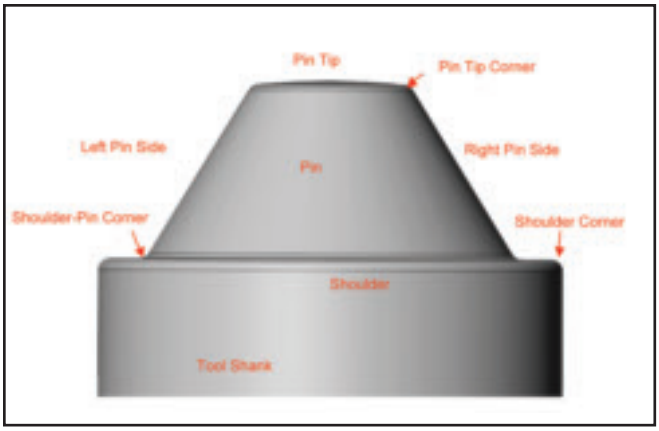

Fig. 1 — Schematic displaying typical tool geometry designations.

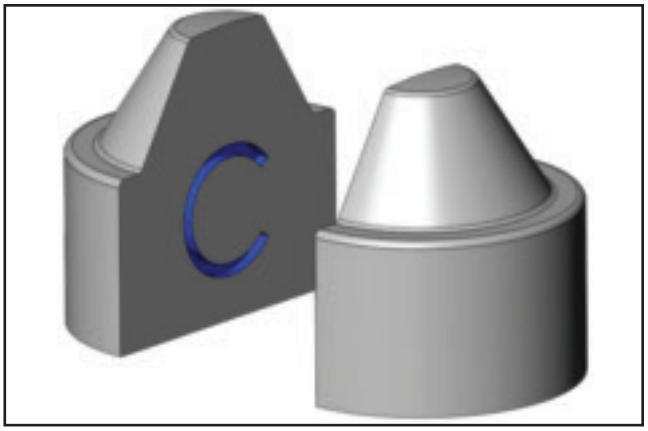

Fig. 2 — Schematic displaying pin tip cross section for postweld inspection.

due to both solid-solution strengthening and grain size refinement. Elevated temperature properties of W-Re have been measured at 1926°C (3498°F) and were shown to be 143 MPa (21 ksi) for ultimate tensile strength (UTS) with a total elongation of 6% (Refs. 9–11).

Material C stands out from Material B because it has an addition of hafnium carbon (HfC) particles. Material C has a specific composition of 70% W, 20% Re, and 10% HfC. This HfC addition has a significant impact on the high-temperature strengths. At 1926°C (3498°F), an alloy with an addition of 2% HfC saw an increase in UTS to approximately 275 MPa or 40 ksi. The addition of the HfC particles to the alloy effectively prevents any grain boundary separation due to plastic deformation at high temperatures. However, these HfC particles decrease the elongation and cause the material to be very brittle at low temperatures. The addition of HfC particles also slows down the recrystallization of the alloy leading to a very fine grain microstructure (Refs. 9, 12, 13).

Each material was acquired in 4-in.- (102-mm-) long, 1.2-in.- (30-mm-) diameter bars and was cut into two sections. The first section was 3 in. (76 mm) long and was machined into a variable-penetration tool (VPT) design (U.S. Patent Nos. 7,234,626, 7,404,510, and 7,416,102). A tool design schematic referencing important pin tool locations is displayed in Fig. 1. The second section was 1 in. (25 mm) long and was cut into two pieces along the central axis. The two resulting pieces were then mounted and polished; one piece being mounted in the cross-section orientation and the other piece being mounted in the traverse orientation. These six mounts were then used for base metal characterization.

A high-strength steel (HSS), nominally 80 ksi or 550 MPa, was chosen as the material to be welded for this study. The plates were approximately 7.5 in. (190 mm) wide, 24.75 in. (629 mm) long, and 0.75 in. (19 mm) thick. The plates were prepared for welding by a machining pass to remove the mill scale and an acetone wipe.

Welding Process

Prior to welding, each tool was characterized dimensionally using digital profilometry and height gauge measurements. The digital profilometry system involved a laser attached to motorized, linear X-Y slides, which move the laser over the part during laser scanning. The laser used to scan the tools was a Micro Epsilon 2800 with Y and Z direction resolution of 0.0009 in. (23 μm).

All three tool material types were welded using the exact same parameters and processing conditions. The welds were completed in position control with a spindle speed of 90 rev/min, a travel speed of 3.5 in./min (89 mm/m), and a travel distanced of 15 in. (381 mm). Typical plunge loads reached a peak of nominally 25,000 lbf (111 kN). These parameters were selected to achieve a cold welding condition that would be more likely to cause degradation of the tools. All welding was performed without primary or secondary shielding.

Postweld Investigation Technique

Postweld, each tool was again characterized dimensionally using the same digital profilometry and height gauge measurements. Each tool was then sectioned in the same manner and prepared for metallographic examination. The first cut was made perpendicular to the central axis just above the shoulder of the tool. A second cut was made along the central axis of the resulting tool tip from the first cut, effectively cutting it in half — Fig. 2. One half of this cut was mounted and polished in preparation for scanning electron microscope (SEM) and optical analysis. Typical SEM parameters included a voltage of 20.00 kV and a probe current of 100 pA.

The SEM was used to examine both the pin tip surface and the mounted cross section of each tool. For investigating the surface, backscatter imaging, secondary imaging, and energy-dispersive X-ray spectrometry (EDS) were employed. The primary areas of interest included pure tool material areas, mixed composition areas (tool material and steel), pin tip surface, pin side surfaces, and shoulder surfaces. When investigating the mounted cross sections of each pin tool, backscatter imaging, secondary imaging, and EDS were also used. The primary areas of interest for the cross sections included the tool shank, tool edge, pin tip edge, pin edge, shoulder edge, and center of the pin. Optical analysis of each mount for selected areas was also performed. Grain size measurements were completed by optically examining one of the

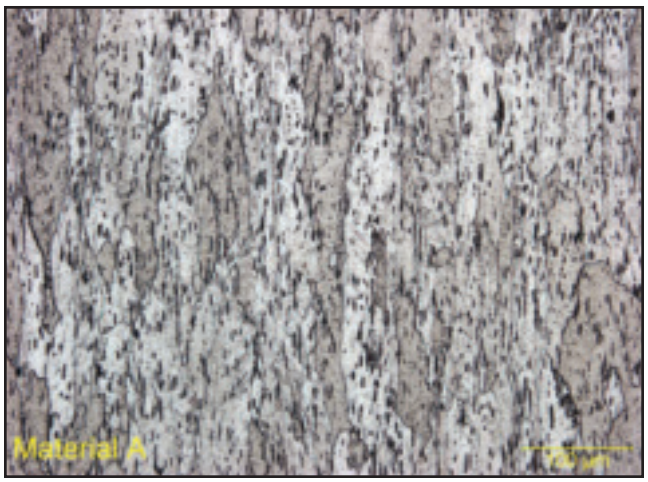

Fig. 3 — Material A raw stock microstructure.

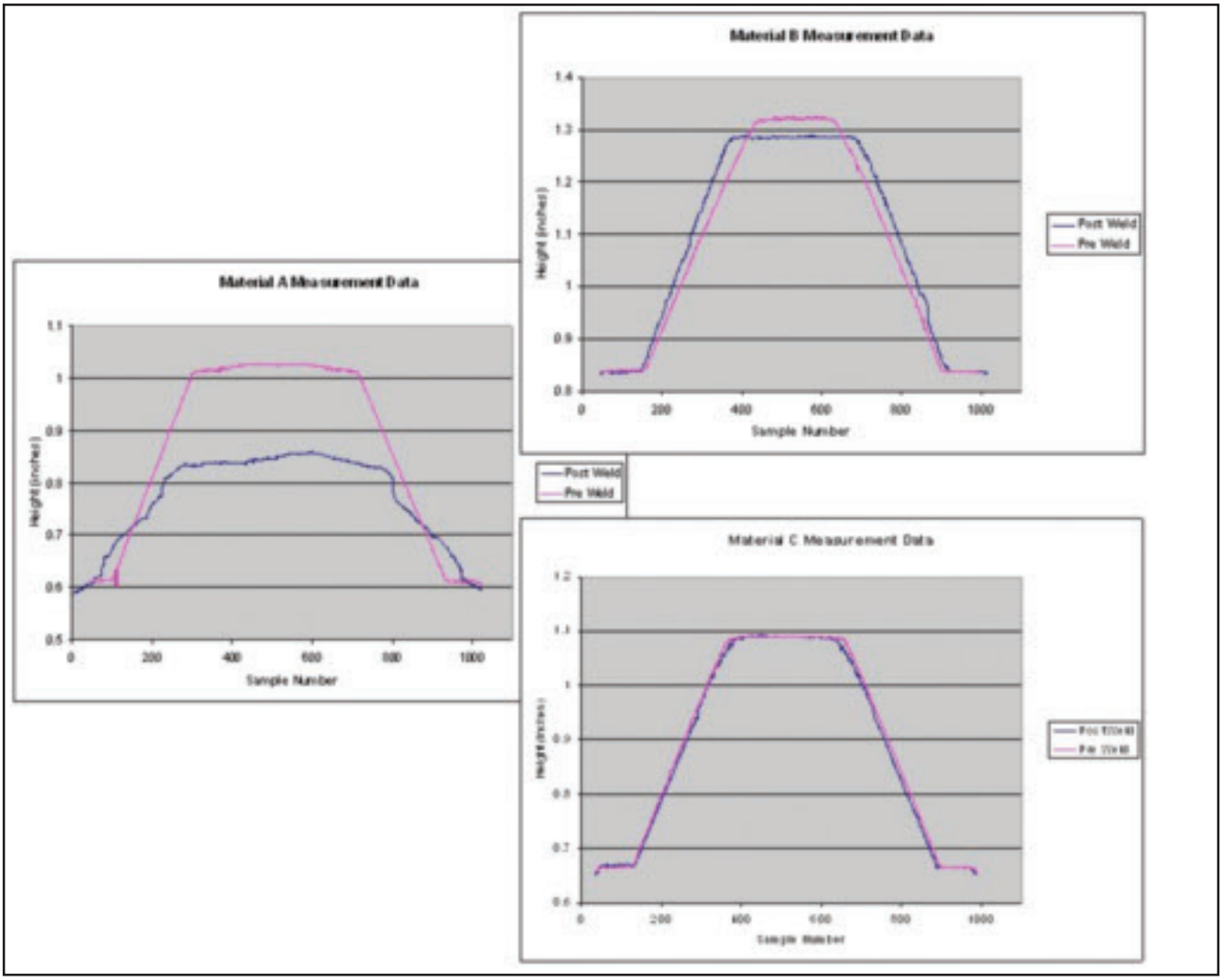

Fig. 4 — Digital profilometry data for each material, pre- and postweld.

selected areas. Two lines were superimposed on a single grain at 90 deg to one another generating a length and width measurement for an individual grain through scale comparison. Average grain size was calculated by averaging individual grain size measurements taken within a 100-μm square area.

Results and Discussion

Characterization of Degradation Mechanisms in Tool Material A (W-La)

The raw stock of Material A is characterized by long vertical grains running parallel to the central axis. Average grain size is approximately 0.006 in. (150 μm) long and 0.002 in. (50 μm) wide — Fig. 3. When welding with this material, the tool visually deformed especially during the plunge sequence. As the tool traversed down the weld, it progressively mushroomed until the original shape was no longer recognizable. Upon retraction, the tool was visibly inspected and the severity at which it had become deformed was confirmed. The tool was also covered with a thick layer of steel extending from the pin tip up to the shoulder.

The digital profilometry data confirmed the pin length was shortened by 0.141 in. (4 mm). The shoulder diameter increased by 0.110 in. (3 mm) and the pin tip diameter increased by 0.100 in. (3 mm). In short, this tool had been compressed in length and expanded outward in diameter confirming a high-stress environment — Fig. 4.

Several instances of deformation were observed during the SEM and optical analysis of this tool material. Many areas of the tool surface showed plastic deformation as well as cracking. Observations of the mounted cross sections revealed further tool degradation in the microstructure, primarily in the form of deformation. Severe deformation of the pin tip and shoulder diameters occurred as well as compression of the pin length. The long grains characteristic of the stock material were twisted and compressed into different orientations. Some of these grains were twisted as much as 90 deg from the original orientation — Fig. 5.

Large areas of recrystallization were also noticed on both sides of the pin tip — Fig. 6. Material A (T_m of 3473 K) has a recrystallization temperature of 1873 K (Ref. 14), while typical temperatures during the FSW of steel reach approximately 900° to 1100°C (1173 to 1373 K) (Ref. 4). Recrystallization cannot occur in this material at FSW temperatures alone. Therefore, it is concluded that the combination of high temperatures and local deformation drove the recrystallization process to occur at a lower temperature.

Abrasive and adhesive wear were also observed; however, the abrasive wear appeared to have a minimal effect. Evidence of the W and steel materials alloy-

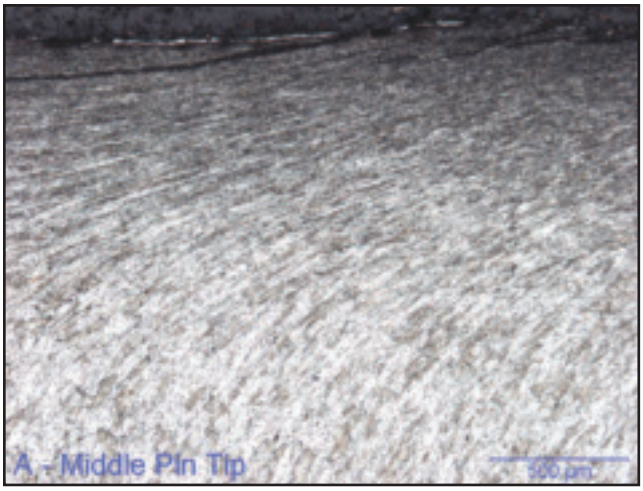

Fig. 5 — Deformed W-La grains at the pin tip.

Fig. 6 — Recrystallized area in W-La pin tip.

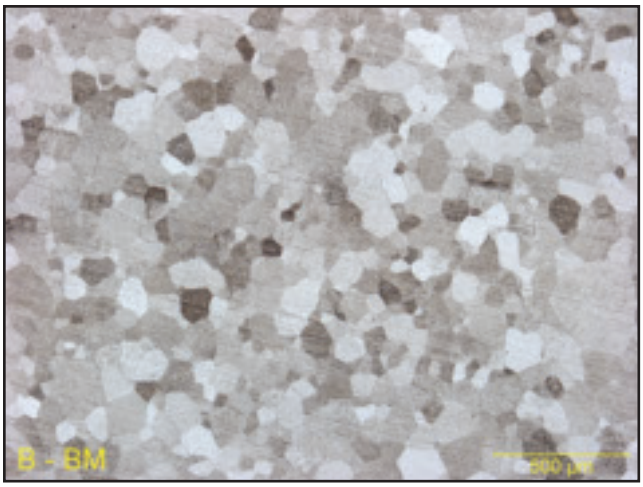

Fig. 7 — Material B raw stock microstructure.

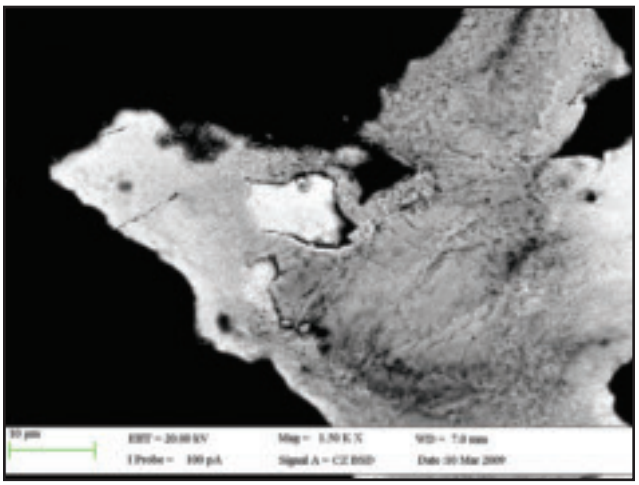

Fig. 8 — SEM backscatter image of Material B tool surface.

ing was also uncovered and could be possible because of the stresses and temperatures the tool material experienced during welding.

In summary, the primary tool degradation mechanism for Material A (W-La) is deformation. It appears that the grain structure was not able to withstand the high stresses experienced during welding and resulted in plastic strain causing the tool to deform from its original shape. In addition, the recrystallization of the material further decreases the ability of the tool to sustain the process loads during welding. These two factors contributed to the tool deforming under compression, causing mushrooming and loss of pin length.

Characterization of Degradation Mechanisms in Tool Material B (W-Re)

The raw stock of Material B is characterized by a fine grain structure, width of 0.004 in. (100 μm) or less, throughout the majority of the material and especially in the center of the bar — Fig. 7. Toward the edge of the bar the grains become quite large, on the order of five times larger (approximately 0.02 in. or 500 μm in width). This large grain region is approximately 0.178 in. (5 mm) wide at each edge. The cause of this difference in grain size is attributed to the material-processing conditions, and as a result, the grains have experienced recrystallization and growth. There are also indications of a possible second phase, most likely W-Re, along the grain boundaries of these larger grains.

During welding, Material B visually showed no signs of deformation or wear. Upon retraction, the tool was visually inspected and there was a light coating of steel on the pin with some slight deformation. Digital profilometry verified the pin length decreased by approximately 0.033 in. (838 μm) and the shoulder diameter increased by approximately 0.006 in. (152 μm). The pin tip diameter saw the largest change with an increase in size of approximately 0.036 in. (914 μm) — Fig. 4.

Investigation of the pin surface using the SEM revealed several instances of material deformation along with cracking, and abrasive and adhesive wear — Fig. 8. SEM analysis and optical microscopy of the pin tip cross section revealed further evidence of degradation. The grains experienced deformation in the form of twinning with subsequent changes in the tool geometry — Fig. 9. Twinning is known to be a natural process associated with increased strength levels and limited slip systems in BCC materials (Ref. 8). These effects were most prominent along the edges of the tool.

The twinning was also observed to initiate cracking, although the number of these cracks was very low — Fig. 10. While this material appears to have twinned in several locations, the occurrence must not be sufficient enough to cause severe cracking. The large grains on the outside edges of the tool were more susceptible to twinning, leading to faster shoulder wear and deformation as compared to the pin tip.

The grains throughout the entire pin experienced some degree of twinning, lesser near the center (25 twins per 0.02 in. or 508 μm square) and base of the pin tip and more severe near the pin and shoulder edges (50 twins per 0.02 in. or 508 μm

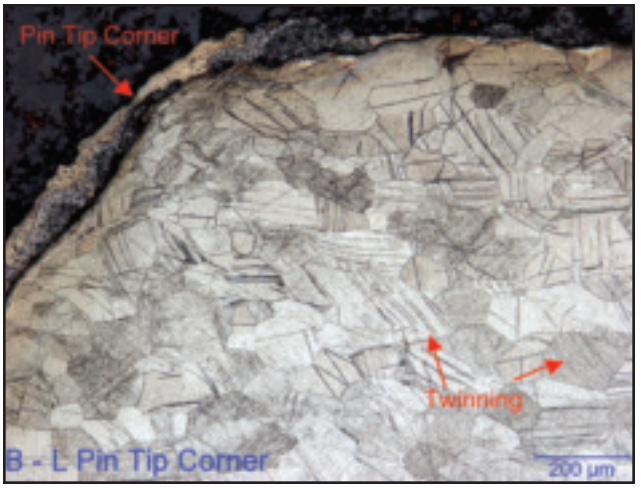

Fig. 9 — Twinning in Material B near pin tip.

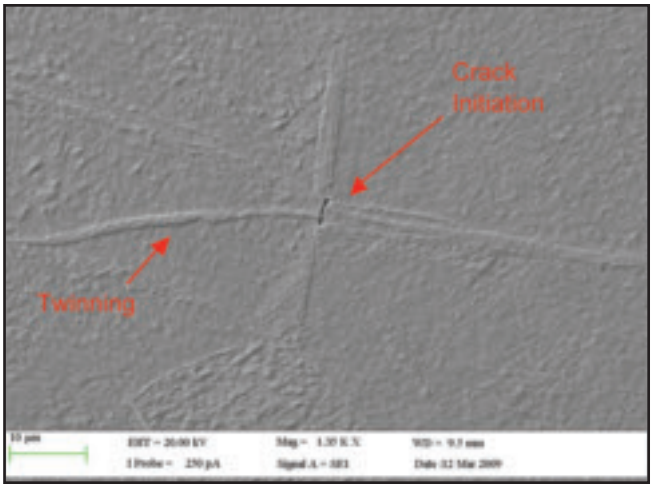

Fig. 10 — Twinning in Material B leading to crack initiation.

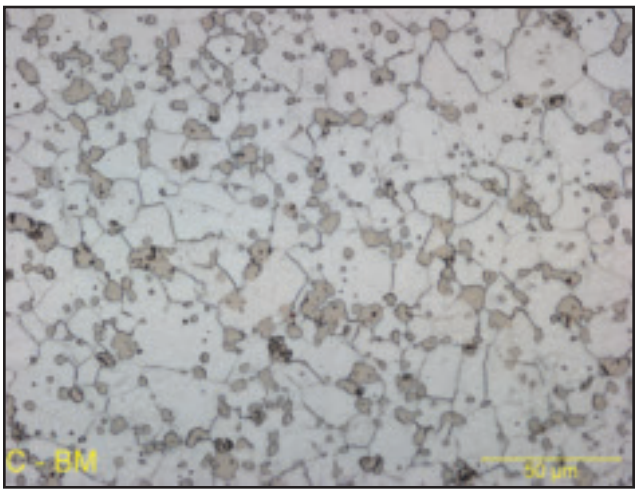

Fig. 11 — Material C raw stock microstructure.

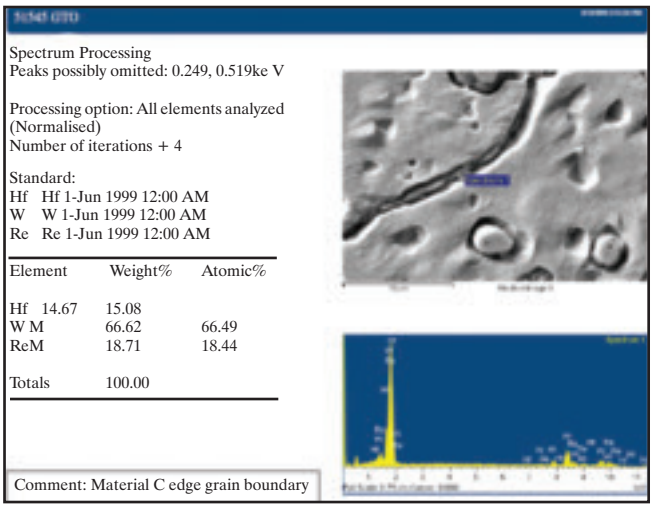
Spectrum Processing
Peaks possibly omitted: 0.249, 0.519ke V

Processing option: All elements analyzed (Normalised)
Number of iterations + 4

Standard:
Hf Hf 1-Jun 1999 12:00 AM
W W 1-Jun 1999 12:00 AM
Re Re 1-Jun 1999 12:00 AM

Element	Weight%	Atomic%
Hf 14.67	15.08	
W M	66.62	66.49
ReM	18.71	18.44
Totals	100.00	

Comment: Material C edge grain boundary

Fig. 12 — EDS analysis of grain boundary separation in Material C.

square). In the end, twinning was seen as the main cause of degradation in Material B. The twinning behavior was not uniform throughout the tool. It is believed this variation in behavior is related to different stress levels throughout the tool during FSW. Material B performed better than Material A due to the addition of Re. The Re significantly increases the strength and ductility of the material at higher temperatures due to solid-solution strengthening and grain refinement. Additionally, the Re raises the recrystallization temperature to 1900°C (3452°F) (Ref. 9).

Characterization of Degradation Mechanisms in Tool Material C (W-Re-HfC)

The raw stock of Material C has a very refined microstructure. Typical grain size was 0.001 in. (25 µm) wide for the W-Re grains and 0.0005 in. (3 µm) wide for the HfC particles — Fig. 11. The HfC particles were located both on the grain boundaries and inside of the W-Re grains. This material also exhibited a surfacing effect on the bar stock that occurred during the processing of the material. This surfacing effect was a layer approximately 0.06 in. (2 mm) wide, and is characterized by separation between the individual W-Re grains. EDS analysis was conducted in the separation area of a typical grain boundary. The analysis showed the region is comprised of W-Re-HfC in approximately the same compositions as the base material — Fig. 12. The occurrence of this grain separation drops off rapidly as the central axis of the tool is approached.

Material C showed very little degradation during welding. After welding, the pin was covered in a very thin layer of steel. Of all three tool materials, Material C was the most resistant to tool degradation. The pin length shortened only by 0.001 in. (25 µm), the shoulder diameter increased by only 0.002 in. (50 µm), and the pin tip diameter increased by 0.0045 in. (114 µm). As with the previous tool materials, the degradation shortened the pin length and mushroomed the pin tip and shoulder — Fig. 4.

Material C raw stock underwent very similar processing as Material B and, as such, has a similar microstructure with one exception, the grain size is much smaller. The HfC particles found both on the grain boundaries and inside the W-Re grains effectively stabilized the W-Re grains during recrystallization. This retarded the grain growth and led to a very refined microstructure. An edge effect of separated grains, approximately 0.06 in. (2 mm) wide, was observed around the outside diameter of the material. This decohesion may be caused by induced residual stresses that occurred when the material was produced.

SEM investigation of the pin surface revealed individual W particles scattered throughout the steel coating in addition to abrasive and adhesive wear. SEM analysis and optical microscopy of the cross section further confirmed the tool material was "breaking off" rather than deforming — Fig. 13. These localized intergranular fracture events appear due to the presence of

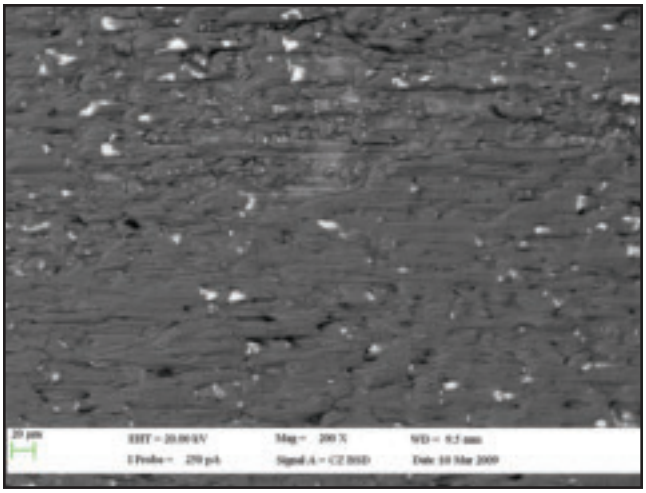

Fig. 13 — Material C pin surface with W particles broken off.

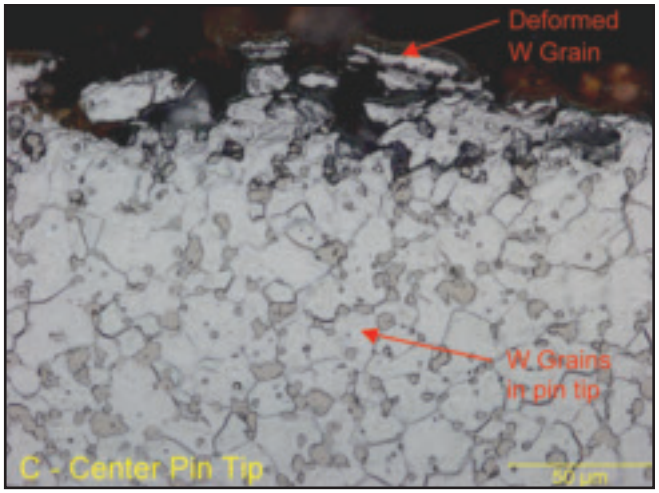

Fig. 14 — Intergranular failure in Material C pin tool.

the HfC particles. The HfC particles effectively prevent softening of the tool material allowing high stresses to develop. This helps to prevent the types of deformation that leads to gross deformation as observed in Materials A and B.

Although the HfC particles provide a significant benefit, they do embrittle the microstructure. As described above, this results in numerous cracks along grain boundaries. This allows pieces of the tool material to be broken away from the tool. Once the W-Re grains are separated from their supporting HfC particles, they begin to deform — Fig. 14.

Material C also showed grain boundary decohesion near the outer diameter of the bar. This decohesion served to exacerbate intergranular failure on the outer corners of the shoulder. These grains were already beginning to separate in the as-received material and the added stress induced by the welding process accelerated their fracture.

The primary tool degradation mechanism of Material C is intergranular failure. Further tool material loss comes from abrasive and adhesive wear. Material C saw very little deformation as the HfC particles supported the surrounding W-Re grains. Material was lost from the tool because the HfC particles acted as cracking paths around the W-Re grains leading to intergranular failure. Once these grains were separated from the HfC particles, they broke off into the weld metal or deformed. Finally, the grain separation on the outer edges of this material helped to promote the intergranular cracking.

Conclusions

The degradation mechanisms of FSW tools made from three separate material types were identified. These mechanisms have been characterized for welding HSS under conditions that would promote tool degradation. For each tool material, the observed degradation was characterized in terms of wear and deformation. This characterization was based upon the inspection of the pre- and postweld tool material microstructures using optical microscopy and SEM. Specific conclusions from this study include the following:

- Tool degradation can be divided into two main categories, deformation and wear
- Material processing plays a significant role in a material's ability to resist tool degradation
- Deformation of the grains provided the most significant source of tool degradation
- Tool materials listed by performance — Materials C, B, and A
- The primary degradation mechanism of Material A was deformation
- The primary degradation mechanism of Material B was twinning
- The primary degradation mechanism of Material C was intergranular failure.

Acknowledgments

EWI acknowledges the contribution of the state of Ohio, Department of Development and Thomas Edison Program, which provided funding in support of Edison Technology and Industry Center Services. In addition, EWI acknowledges the contributions of Rhenium Alloys, Inc., to this project.

References

1. Klingensmith, S., DuPont, J. N., and Marder, A. R. 2005. Microstructural characterization of a double-sided friction stir weld on a superaustenitic stainless steel. *Welding Journal* pp. 77–85.

2. Lienert, T. J., Tang, W., Hogeboom, J. A., and Kvidahl, L. G. 2004. Friction stir welding of DH-36 steel. *Joining of Advanced and Specialty Materials VI*, Materials Solutions.

3. Sato, Y. S., Muraguchi, M., and Kokawa, H. 2007. Microstructure and properties of friction stir welded 304 stainless steel using W-based alloy tool. *Friction Stir Welding and Processing IV*, eds. R. S. Mishra, M. W. Mahoney, T. J. Lienert, and K. V. Jata, TMS, pp. 261–268.

4. Gan, W., Li, T., and Khurana, S. 2007. Tool mushrooming in friction stir welding of L80 steel. *Friction Stir Welding and Processing IV*, eds. R. S. Mishra, M. W. Mahoney, T. J. Lienert, and K. V. Jata, TMS, pp. 279–283.

5. Weinberger, T., Kosha, S., Fuhrer, B., and Ensinger, N. 2008. Analysis of tool wear and failure mechanism during friction stir welding of steel. *7th International Friction Stir Welding Symposium*, Session 9B, Awaji Island, Japan.

6. Bentley, A. R., and Hogwood, M. C. 1992. The effect of mechanical deformation and heat treatment on the microstructural characteristics of two tungsten heavy alloys. *Tungsten and Tungsten Alloys Conference*, pp. 419–429.

7. Tucker Jr., R. C. 1997. *Wear Failures. Friction and Wear Testing Source Book: Selected References from ASTM Standards and ASM Handbooks*, ASM International, pp. 168–185.

8. Guy, A. and Hren, J. 1974. *Elements of Physical Metallurgy*, Third Edition, Addison-Wesley Publishing Co., Reading, Mass.

9. Leonhardt, T. 2009. Processing and properties of tungsten 25% rhenium with and without hafnium carbide. Plansee Seminar.

10. Bryskin, B. D., and Carlén, J.-C. 1996. Sigma phase in tungsten-rhenium alloys, I. *Materials and Manufacturing Processes*, Vol. 11, No. 1, pp. 67–81, Marcel Dekker, Inc.

11. German, R. M., and Bose, A. 1991. Properties of high density tungsten-rhenium alloys by liquid phase sintering. *Tungsten and Tungsten Alloys Recent Advances*, eds. A. Crowson and E. S. Chen, TMS, pp. 53–59.

12. Shin, K. S., Luo, A., Chen, B.-L., and Jacobson, D. L. 1990. High-temperature properties of particle strengthened W-Re. *JOM*, pp. 12–15.

13. Tsao, B. H., and Ramalingam, M. L. 1991. The effect of ThO_2 and HfC on the recrystallization of W-Re alloys. *Tungsten and Tungsten Alloys Conference*, New Orleans, La. pp. 17–22.

14. 2009. Tungsten, material properties and applications. Plansee, *www.plansee.com/lib/Tungsten_DE.pdf*.